NeuroImage: Clinical 15 (2017) 428–438

Contents lists available at ScienceDirect

NeuroImage: Clinical

journal homepage: www.elsevier.com/locate/ynicl

Multiparametric MRI to distinguish early onset Alzheimer's disease and behavioural variant of frontotemporal dementia

Elisa Canu[a], Federica Agosta[a], Gorana Mandic-Stojmenovic[a,c], Tanja Stojković[c], Elka Stefanova[c], Alberto Inuggi[d], Francesca Imperiale[a], Massimiliano Copetti[e], Vladimir S. Kostic[c], Massimo Filippi[a,b,*]

[a] Neuroimaging Research Unit, Institute of Experimental Neurology, Division of Neuroscience, San Raffaele Scientific Institute, via Olgettina 60, 20132 Milan, Italy
[b] Department of Neurology, Institute of Experimental Neurology, Division of Neuroscience, San Raffaele Scientific Institute, via Olgettina 60, 20132 Milan, Italy
[c] Clinic of Neurology, Faculty of Medicine, University of Belgrade, Dr Subotića 6, PO Box 12, 11129 Belgrade 102, Serbia
[d] Unit of Robotics, Brain and Cognitive Sciences, Istituto Italiano di Tecnologia, Via Morego, 30, 16163 Genoa, Italy
[e] Biostatistics Unit, IRCCS-Ospedale Casa Sollievo della Sofferenza, Viale Cappuccini, San Giovanni Rotondo, 71013 Foggia, Italy

ARTICLE INFO

Keywords:
Early onset Alzheimer's disease
Behavioural variant of frontotemporal dementia
Diagnosis
Cortical thickness
White matter (WM) damage
Resting state functional MRI

ABSTRACT

This prospective study explored whether an approach combining structural [cortical thickness and white matter (WM) microstructure] and resting state functional MRI can aid differentiation between 62 early onset Alzheimer's disease (EOAD) and 27 behavioural variant of frontotemporal dementia (bvFTD) patients. Random forest and receiver operator characteristic curve analyses assessed the ability of MRI in classifying the two clinical syndromes. All patients showed a distributed pattern of brain alterations relative to controls. Compared to bvFTD, EOAD patients showed bilateral inferior parietal cortical thinning and decreased default mode network functional connectivity. Compared to EOAD, bvFTD patients showed bilateral orbitofrontal and temporal cortical thinning, and WM damage of the corpus callosum, bilateral uncinate fasciculus, and left superior longitudinal fasciculus. Random forest analysis revealed that left inferior parietal cortical thickness (accuracy 0.78, specificity 0.76, sensitivity 0.83) and WM integrity of the right uncinate fasciculus (accuracy 0.81, specificity 0.96, sensitivity 0.43) were the best predictors of clinical diagnosis. The combination of cortical thickness and DT MRI measures was able to distinguish patients with EOAD and bvFTD with accuracy 0.82, specificity 0.76, and sensitivity 0.96. The diagnostic ability of MRI models was confirmed in a subsample of patients with biomarker-based clinical diagnosis. Multiparametric MRI is useful to identify brain alterations which are specific to EOAD and bvFTD. A severe cortical involvement is suggestive of EOAD, while a prominent WM damage is indicative of bvFTD.

1. Introduction

Early onset Alzheimer's disease (EOAD) and behavioural variant frontotemporal dementia (bvFTD) are the most common types of presenile neurodegenerative dementia (*i.e.*, age at onset of 65 years of younger) (Picard et al., 2011). Compared to the typical episodic memory dysfunction of late onset AD (LOAD), EOAD patients show a constellation of multi-domain deficits at presentation which can include memory, but also language, executive, visuospatial abnormalities and behavioural disturbances similar to those manifested by bvFTD cases (Smits et al., 2012). BvFTD typically presents with marked changes in personality, such as socially inappropriate and impulsive behavior, diminished social interest and apathy, and with a cognitive profile characterized by executive dysfunctions, such as impairment in problem solving and inhibitory control (Rascovsky et al., 2011). However, bvFTD can have a very heterogeneous presentation with some patients presenting with difficulties in memory recall or in visuospatial abilities (Rascovsky et al., 2002).

Although clinical criteria have the potential to increase diagnostic accuracy (McMillan et al., 2013), the frequent overlap of clinical

Abbreviations: ACE-R, Addenbrooke's Cognitive Examination-revised; EOAD, early onset Alzheimer's disease; bvFTD, behavioural variant frontotemporal dementia; CSF, cerebrospinal fluid; CC, corpus callosum; DMN, default mode network; DT, diffusion tensor; GM, grey matter; IC, independent component; ILF, inferior longitudinal fasciculus; LOAD, late onset Alzheimer's disease; MNI, Montreal Neurological Institute; NVI, Normalized Variable Importance; RS fMRI, resting state functional MRI; RSN, resting state network; SLF, superior longitudinal fasciculus; TFCE, threshold-free cluster enhancement; WM, white matter

* Corresponding author at: Neuroimaging Research Unit, Institute of Experimental Neurology, Division of Neuroscience, San Raffaele Scientific Institute, Vita-Salute San Raffaele University, Via Olgettina, 60, 20132 Milan, Italy.
E-mail address: filippi.massimo@hsr.it (M. Filippi).

http://dx.doi.org/10.1016/j.nicl.2017.05.018
Received 7 March 2017; Received in revised form 12 May 2017; Accepted 25 May 2017
Available online 25 May 2017

symptoms associated with EOAD and bvFTD poses serious problems in the differential diagnosis with the consequence that they are frequently misdiagnosed, even in the most expert centers. A number of studies showed that several path-proven AD patients received *in vita* a diagnosis of bvFTD, or vice versa, with the majority of misclassified cases having an early age of onset and/or neuropsychiatric symptoms (Alladi et al., 2007; Harris et al., 2013; Mendez et al., 2013; Rabinovici et al., 2007; Rascovsky et al., 2011). In these cases, the current amyloid markers can be helpful (Jack et al., 2016). However, they are not always available in the clinical practice due to the high costs of the procedures. In addition, when present and positive, they might not reflect the primary underneath pathology (Caso et al., 2013; Serrano et al., 2014). Thus, there is a strong need for additional markers of brain changes associated with the two types of neurodegenerative disorder. Among the most available instrumental tools, magnetic resonance imaging (MRI) is promising in detecting structural and functional brain differences between these two patient populations.

Volumetric and cortical thickness studies have shown a prevalent involvement of posterior parietal regions in EOAD and of anterior fronto-insular-striatal areas in bvFTD (Du et al., 2007; Rabinovici et al., 2007). A number of studies reported a greater white matter (WM) involvement in bvFTD compared to EOAD (Lu et al., 2014; Mahoney et al., 2014; McMillan et al., 2012; Moller et al., 2015; Zhang et al., 2011; Zhang et al., 2009). Finally, resting state functional MRI (RS fMRI) studies observed a divergent pattern of altered functional connectivity in the default mode network (DMN) and salience network comparing EOAD and bvFTD patients (Filippi et al., 2013; Zhou et al., 2010).

The aims of this multiparametric MRI study were to explore whether an approach combining structural (cortical thickness and WM microstructure) and functional (RS fMRI connectivity) brain imaging can be useful in differentiating EOAD and bvFTD *in vivo* and to identify which MRI metrics are the best predictors of clinical diagnosis at the individual subject level. If successful, this approach has the potential to be powerful also when applied to rare AD conditions, such as the frontal variant of AD (Johnson et al., 1999), which mimic the bvFTD, in terms of frontal lobe functioning, due to the an unusually high degree of frontal tangle pathology at autopsy.

2. Methods

2.1. Participants

Sixty-two patients with a diagnosis of probable AD (McKhann et al., 2011) and age of onset < 65 years, 27 patients with a diagnosis of bvFTD (Rascovsky et al., 2011) and matched with AD cases for age at onset and disease duration, and 48 age-matched healthy controls were recruited consecutively at the Clinic of Neurology, Faculty of Medicine, University of Belgrade, Serbia. According to established criteria (McKhann et al., 2011; Rascovsky et al., 2011), the patient diagnoses were based on a comprehensive evaluation including clinical history, neurological examination, and neuropsychological testing. An experienced neurologist blinded to the MRI results performed clinical assessments. Eligibility criteria included: no family history of dementia; no significant medical illnesses or substance abuse that could interfere with cognitive functioning; any other major systemic, psychiatric or neurological illnesses; and absence of other causes of focal or diffuse brain damage, including lacunae and extensive cerebrovascular disease at routine MRI. When available, clinical diagnoses were confirmed by 18F-2-fluoro-2-deoxy-D-glucose positron emission tomography (38 EOAD and 24 bvFTD patients) and/or cerebrospinal fluid (CSF) biomarkers (24 EOAD and 9 bvFTD patients). Atypical focal presentations of AD (*i.e.*, logopenic variant of primary progressive aphasia and posterior cortical atrophy) were not included. Healthy controls with no history of neurologic, psychiatric or other major medical illnesses were recruited among friends and spouses of patients and by word of mouth. This prospective study was approved by the Local Ethical Committee on human studies and written informed consent from all subjects (or their legal guardians) was obtained prior to their enrolment.

2.2. Neuropsychological assessment

Neuropsychological and behavioural evaluations were completed within 48 h of MRI by an experienced neuropsychologist, who was unaware of the MRI data. The assessment evaluated global cognition with the Mini-Mental State Examination (Folstein et al., 1975), the Addenbrooke's Cognitive Examination-revised (ACE-R) (Mioshi et al., 2006), and the Frontal Assessment Battery (Dubois et al., 2000). Memory was investigated with the Rey Auditory Verbal Learning Task (Johnson et al., 1999), the Free and Cue Selective Reminding Test (Grober and Buschke, 1987), the Wechsler Memory Scale (Wechsler, 1987), and the digit span forward (Wechsler, 1987). The phonemic (Benton, 1968) and the semantic fluencies (Kim et al., 2007), the digit span backward (Wechsler, 1987), the digit ordering test (maximal span) (Cooper et al., 1991), the digit symbol (Wechsler, 1987), and the Stroop test (correct answers) (Sajjadi et al., 2013) were used to test executive functions. The language domain was assessed with the Boston Naming Test (Kim et al., 2007), and the Boston Diagnostic Aphasia Examination (Kim et al., 2007). The Clock drawing test (Rowe et al., 2010), the Hooper Visual Organization test (Villemagne et al., 2014), and the visual spatial sub-test of the ACE-R (Mioshi et al., 2006) were chosen to investigate the visuospatial domain. Furthermore, mood was evaluated with the Hamilton Depression Rating Scale (Villemagne and Okamura, 2014), the Hamilton Anxiety Rating scale (Dani et al., 2016), and the Apathy Evaluation Scale (Passamonti et al., 2017). Behavioural disturbances were investigated using the Neuropsychiatric Inventory (Cummings et al., 1994) with the patient caregiver.

2.3. MRI acquisition

MRI scans were obtained on a 1.5 Tesla Philips Medical System Achieva scanner. The following sequences were acquired: (i) dual-echo turbo spin-echo (repetition time [TR] = 3125 ms, echo time [TE] = 20/100 ms, echo train length = 6, 44 axial slices, thickness = 3 mm with no gap, matrix size = 256 × 247, field of view [FOV] = 240 × 232 mm^2); (ii) three-dimensional (3D) sagittal T1-weighted Turbo Field Echo (TFE) (frequency direction = anterior-posterior; TR = 7.1 ms, TE = 3.3 ms, inversion time = 1000 ms, flip angle = 8°, matrix size = 256 × 256 × 180 [inferior-superior, anterior-posterior, left-right], FOV = 256 × 256 mm^2); (iii) pulsed gradient SE single shot echo-planar (TR = 6715 ms, TE = 86 ms, flip angle = 90°, matrix size = 112 × 110, FOV = 224 × 220 mm^2; 50 axial slices, thickness = 2.6 mm with no gap), with diffusion-encoding gradients applied in 65 non-collinear directions, selected as the default in the scanner (b factor = 1000 s/mm^2; seven averages). The maximum amplitude of the diffusion gradients was 33 mT/m and a multiple channel head coil was used for signal reception; and (iv) gradient-echo (GRE) echo planar imaging (EPI) for RS fMRI (TR = 3000 ms, TE = 35 ms, flip angle = 90°, matrix size = 128 × 128, FOV = 240 × 240 mm^2; slice thickness = 4 mm, 200 sets of 30 contiguous axial slices). Total acquisition time of RS fMRI was about 12 min. During scanning, subjects were instructed to remain motionless and to keep their eyes closed.

2.4. MRI analysis

2.4.1. Cortical thickness

Cortical reconstruction and estimation of cortical thickness were performed on the 3D T1-weighted TFE images using the FreeSurfer image analysis suite, version 5.3 (http://surfer.nmr.mgh.harvard.edu/) (Fischl and Dale, 2000). After registration to Talairach space and intensity normalization, an automatic skull stripping was performed, which removes extra-cerebral structures, cerebellum and brainstem, by

using a hybrid method combining watershed algorithms and deformable surface models. Images were then carefully checked for skull stripping errors, and segmented into grey matter (GM), WM, and CSF. Then, cerebral hemispheres were separated, and subcortical structures divided from cortical components. The WM/GM boundary was tessellated and the surface was deformed following intensity gradients to optimally place WM/GM and GM/CSF borders, thus obtaining the WM and the pial surfaces (Dale et al., 1999). The results of this segmentation procedure were inspected visually, and if necessary, edited manually by adding control points. Afterwards, surface inflation and registration to a spherical atlas were performed (Dale et al., 1999) and the cerebral cortex parcellated into 34 regions per hemisphere, based on gyral and sulcal structures, as described by Desikan et al. (2006). Finally, cortical thickness was estimated as the average shortest distance between the WM boundary and the pial surface.

2.4.2. WM microstructure

The diffusion-weighted data were skull-stripped using the Brain Extraction Tool implemented in FSLv5.0 (http://fsl.fmrib.ox.ac.uk/fsl). Diffusion-weighted images were corrected for distortions caused by eddy currents and movements, using an implementation of the algorithm described in Rohde et al., 2004 (Rohde et al., 2004). The diffusion tensor (DT) was estimated on a voxel-by-voxel basis using the DTIfit toolbox, part of the FMRIB Diffusion Toolbox within FSL, in order to obtain fractional anisotropy (FA), mean diffusivity (MD), axial diffusivity (axD), and radial diffusivity (radD) maps. To investigate WM microstructure, we first run tract-based spatial statistics (TBSS) in order to provide a voxel-wise overview of the patterns of WM damage in patient groups compared to controls and each other. However, TBSS does not provide continue variables to be used in the classification analysis. On the other hand, the mean tract DT MRI values are optimal for such an approach. Thus, TBSS findings guided the subsequent tractography analysis by driving the selection of tracts of interest involved in EOAD and bvFTD when compared to each other together with spared tracts used as control condition. Details of the preprocessing related to each of these approaches are described in the following paragraphs.

2.4.3. TBSS

Tract-based spatial statistics (TBSS) version 1.2 (http://fsl.fmrib.ox.ac.uk/fsl/fslwiki/TBSS) was used to perform the multi-subject DT MRI analysis (Smith et al., 2006). FA volumes were aligned to a target image using the following procedure: (i) the FA template in standard space was selected as the target image; (ii) the non-linear transformation that mapped each subject's FA to the target image was estimated using the FMRIB's Non-linear Image Registration Tool (FNIRT); and (iii) the same transformation was used to move each subject's FA to the standard space. A mean FA image was then created by averaging the aligned individual FA images, and thinned to create an FA skeleton representing WM tracts common to all subjects (Smith et al., 2006). The FA skeleton was thresholded at a value of 0.2 to exclude voxels with low FA values, which are likely to include GM or CSF. Individual FA, MD, axD, and radD data were projected onto the common skeleton.

2.4.4. Tractography

Seeds for tractography of the cingulum (split in the anterior cingulum and parahippocampal tract), corpus callosum (CC whole tract, as well as genu, body and splenium), superior longitudinal (SLF), inferior longitudinal (ILF), uncinate fasciculi and corticospinal tract were defined in the Montreal Neurological Institute (MNI) space on the FA template provided by FSL, as previously described (Canu et al., 2015). Fiber tracking was performed in native DT MRI space using a probabilistic tractography algorithm implemented in FSL (probtrackx), which is based on Bayesian estimation of diffusion parameters (Bedpostx) (Behrens et al., 2007). Fiber tracking was initiated from all voxels within the seed masks in the diffusion space to generate 5000 streamline samples with a step length of 0.5 mm and a curvature threshold of 0.2. Tract maps were then normalized taking into consideration the number of voxels in the seed masks. To this aim, the number of streamlines present in the voxels of the tract maps was divided by the way-total, which corresponds to the total number of streamlines that were not rejected by the exclusion masks. The tract masks obtained were thresholded at a value equal to 40% of the 95th percentile of the distribution of the intensity values of the voxels included in the tract. This normalization procedure allowed to correct for possible differences between tracts due to the different sizes of the starting seeds. In this way, we also excluded the background noise and avoided a too restrictive thresholding when the maximum intensity value was an outlier. Using a "seed" approach, the reconstructions of the tracts of interest were obtained. For each tract, the average FA, MD, axD and radD were calculated in the native space.

2.4.5. Resting state functional connectivity

FMRI analysis was performed using FSL (FSLv5.0). Preprocessing was performed using FEAT (Jenkinson et al., 2012; Smith et al., 2004; Woolrich et al., 2009) and included: (i) removal of the first four volumes to allow for signal equilibration; (ii) head movement correction by volume-realignment to the middle volume using MCFLIRT: (iii) global 4D mean intensity normalization; and (iv) spatial smoothing (5 mm FWHM). We then applied ICA-AROMA (Independent Component Analysis-based Automatic Removal Of Motion Artifacts) (Pruim et al., 2015) in order to identify those independent components (ICs) representing motion-related artifacts. This method calculates a set of spatial and temporal discriminative features and, according to them, exploits a classification procedure to identify ICs representing motion artifacts. Specifically, these features evaluate the spatial overlaps of each component with the edges of brain and CSF, and the frequency content and the temporal correlation with realignment parameters of the IC time-series. Finally, ICs classified as motion-related were removed from the fMRI dataset by means of linear regression. Resulting fMRI dataset was then high-pass filtered (cut-off frequency of 0.01 Hz) and co-registered to the participant's 3D T1-weighted TFE image using affine boundary-based registration as implemented in FLIRT (Greve and Fischl, 2009; Jenkinson and Smith, 2001), and subsequently transformed to the MNI152 standard space with 4 mm isotropic resolution using non-linear registration through FNIRT (Andersson et al., 2007). Pre-processed fMRI data, containing 196 time-points for each subject, were temporally concatenated across subjects to create a single 4D dataset. This FMRI dataset was then decomposed into ICs with a free estimation for the number of components using MELODIC (Multivariate Exploratory Linear Optimized Decomposition into Independent Components) (Beckmann et al., 2005).

2.5. Statistical analysis

2.5.1. Demographic, clinical and cognitive data

Normal distribution assumption was checked by means of Q-Q plot and Shapiro-Wilks and Kolmogorov-Smirnov tests. Group comparisons of continuous variables were performed using ANOVA models, followed by post-hoc pairwise comparisons (SAS Release 9.3, SAS Institute, Cary, NC, USA).

2.5.2. Cortical thickness and tractography metrics

Mean cortical thickness and WM tract DT MRI measures were compared between groups using ANOVA models, $p < 0.05$ false-discovery rate (FDR)-corrected for multiple comparisons.

2.5.3. TBSS

TBSS results were assessed using a permutation-based inference tool for nonparametric statistical thresholding ("randomize", part of FSL). FA, MD, axD and radD values within the skeleton were tested between groups using two-sample *t*-tests. The number of permutations was set at

5000. The resulting statistical maps were thresholded at $p < 0.05$, corrected for multiple comparisons at the cluster level using the threshold-free cluster enhancement (TFCE) option.

2.5.4. RS functional connectivity

Between-group analysis of the RS fMRI data was carried out using a dual-regression technique as implemented in FSL (Filippini et al., 2009), an approach that allows to identify subject-specific temporal dynamics and spatial maps that are associated with each group IC map. Among group-IC spatial maps, ICs of interest (sensorimotor, DMN, salience, frontal, fronto-striatal, dorsal attentive, associative and visual networks) were selected by visual inspection based on previous literature (Smith and Nichols, 2009). Then, dual-regression procedure was performed, which involves: (i) the use of the selected group-IC spatial maps in a linear model fit (spatial regression) against the single subject fMRI data sets, resulting in matrices describing temporal dynamics for each IC and subject; and (ii) the use of these time-course matrices which are entered into a linear model fit (temporal regression) against the associated fMRI data set to estimate subject-specific spatial maps (Filippini et al., 2009). After dual regression, spatial maps of all subjects were collected into single 4D files for each original IC. Nonparametric permutation tests (5000 permutations) were used to detect statistically significant differences between groups within the resting state network (RSN) of interest obtained with MELODIC (the single 4D files for each original IC). Furthermore, analyses were restricted within the spatial RSN of interest using binary masks obtained by thresholding the corresponding Z map image ($Z > 2.3$). FWE correction for multiple comparisons was performed, implementing the TFCE method using a significance threshold of $p < 0.05$.

2.5.5. Correlation analysis

In each patient group, correlations between MRI measures (cortical thickness, DT MRI metrics and functional connectivity), cognitive test scores (memory and executive function Z scores) and CSF protein levels (when available) were estimated using Spearman rho coefficient, FDR-corrected for multiple comparisons (SAS Release 9.3).

2.5.6. Discrimination analysis

Using R (randomForest, party-packages), a random forest approach (Breiman, 2001) was applied to identify the MRI measures that best predict the clinical diagnosis (EOAD *vs* bvFTD). Specifically, the random forest was used to model the relationship between the dichotomous outcome "clinical diagnosis" (EOAD *vs* bvFTD) and the multiple potential predictor variables (*i.e.*, MRI metrics), providing information on variable importance. According to the random forest technique (Breiman, 2001), 100.000 trees were built. The training set used to grow each tree is a 0.632 + bootstrap resample of the observations (Efron and Tibshirani, 1997). The best split at each node was selected from a random subset of covariates (*i.e.*, MRI metrics). The left-out observations (*i.e.*, "out of bag" observations) were then predicted to obtain the classification error of the considered tree. The goodness of the fit of the random forest was assessed averaging the individual tree classification errors. Furthermore, the random forest framework estimates the importance of a predictor by looking at how much the classification error increases when out of bag data for that variable are permuted while all others are left unchanged. The variables' importance was ranked by assigning to each covariate a score based on the ability to predict correctly the dependent variable (patient group *vs.* each other) according to the increase of classification error when values of that covariate in a node were permuted randomly. We followed the strategy of Strobl et al. (2007)) to avoid possible biases in variable selection: individual classification trees were built using subsampling without replacement and adopting a conditional permutation scheme to compute variable importance in term of mean decrease in accuracy (*i.e.*, each covariate receives a score according to its ability to classify correctly the patient according to the decrease of classification accuracy) (Strobl et al., 2008). Only those variables that were significantly different between patient groups entered the analysis. The random forest was applied to cortical thickness and tractography measures separately and in combination. The diagnostic performance of the best MRI variables according to the random forest was reported using accuracy, sensitivity and specificity.

2.5.7. Analysis of a sub-sample of patients with CSF and/or PET diagnostic biomarkers

All the analyses described above were applied to a sub-sample of patients having at least one biomarker, among CSF protein levels and FDG-PET, supporting the diagnosis (47 EOAD: 9 with AD-like CSF pattern; 23 with FDG-PET suggestive of AD; 15 with both CSF and PET AD-like biomarkers; 25 bvFTD: 1 with non-AD CSF pattern; 15 with a FDG-PET suggestive of bvFTD; 9 with both CSF and FDG non-AD biomarkers). All 48 healthy controls were included in this analysis.

3. Results

3.1. Demographic, clinical and cognitive data

EOAD patients showed higher scores at the Clinical Dementia Rating scale and lower at the Basic Activity of Daily Living compared to bvFTD cases (Table 1). In the 33 patients who underwent CSF analysis,

Table 1
Demographic and clinical characteristics of patients and healthy controls.

	EOAD	bvFTD	HC	p EOAD *vs* HC	p bvFTD *vs* HC	p EOAD *vs* bvFTD
N	62	27	48			
Age at MRI, years	59.7 ± 4.1 (50–67)	57.7 ± 8.1 (39–70)	57.4 ± 6.3 (49–70)	0.13	1.00	0.41
Age at onset, years	56.2 ± 4.1 (47–65)	53.9 ± 8.6 (32–65)	–	–	–	0.19
Disease duration, years	3.6 ± 1.3 (1–7)	3.8 ± 3.0 (1 – 13)	–	–	–	0.76
Education, years	12.0 ± 2.6 (8–16)	12.3 ± 2.8 (4–18)	13.3 ± 2.8 (8–18)	0.07	0.49	1.00
Gender, women	37 (60%)	11 (41%)	31 (65%)	0.69	0.06	0.11
CDR	1.8 ± 0.8 (1–3)	1.3 ± 0.6 (0–2)	–	–	–	< 0.001
CDR, sb	12.0 ± 4.9 (5–18)	5.6 ± 3.7 (0 – 11)	–	–	–	< 0.001
BADL	41.2 ± 18.9 (4–70)	57.0 ± 14.7 (4–78)	–	–	–	< 0.001
CSF, Aβ42*	419 ± 100 (154–556)	1091 ± 228 (728–1499)	–	–	–	< 0.001
CSF, T-tau*	567 ± 274 (83–1289)	248 ± 104 (78–380)	–	–	–	< 0.001
CSF, p-tau*	82 ± 36 (20–156)	50 ± 21 (21–80)	–	–	–	0.01

Numbers are mean ± standard deviation (range) or frequencies (%). *P* values refer to ANOVA models, followed by post-hoc pairwise comparisons. Abbreviations: Aβ42 = amyloid β42; BADL = Basic Activity of Daily Living; CDR = Clinical Dementia Rating; CDR, sb = Clinical Dementia Rating, sum of boxes; CSF = cerebrospinal fluid; MRI = Magnetic Resonance Imaging; T-tau = total tau; p-tau = phosphorilated tau.

* Data available for 24 EOAD (39%) and nine bvFTD (33%). CSF cut off = Aβ42 < 563.1 ng/L (nanogram/Liter; values below are considered abnormal); T-tau > 244.7 ng/L and p-tau > 83.4 ng/L (values above are considered abnormal).

β-Amyloid 42 levels were lower and total- and phospho-Tau levels were higher in EOAD relative to bvFTD patients (Table 1). Compared to controls, both groups of patients showed worse performances in all cognitive tests, except for the recognition phase of verbal and visual memory tests where bvFTD patients performed similarly to controls (Table A.1). Relative to controls, all patients showed also higher scores at the apathy questionnaire (Table A.1). EOAD patients had greater deficits than bvFTD in all cognitive tests, while bvFTD patients showed more severe behavioural disturbances relative to EOAD cases according to the caregiver reports (Neuropsychiatric Inventory and interviews; Table A.1). Specifically, bvFTD patients reported higher scores of apathy ($p < 0.001$), disinhibition ($p < 0.001$), hyperorality and dietary changes ($p < 0.001$), irritability ($p < 0.001$), aberrant motor behavior ($p < 0.001$), agitation ($p = 0.004$), and euphoria ($p = 0.004$) than EOAD patients.

3.2. Cortical thickness

Compared with controls, bvFTD and EOAD patients showed a widespread pattern of cortical thinning involving all cerebral lobes (Table A.2). Compared to bvFTD, EOAD patients showed cortical thinning of the precuneus, posterior cingulate, superior and inferior parietal, supramarginal, postcentral, and lingual gyri, and lateral occipital cortex bilaterally, and left rostral and caudal middle frontal gyri (Table A.2; Fig. 1). Compared to EOAD, bvFTD patients showed cortical thinning of the lateral orbitofrontal gyrus and temporal pole bilaterally, right medial orbitofrontal gyrus, and right entorhinal cortex (Table A.2; Fig. 1).

3.3. WM microstructure: Tract-based spatial statistics

Compared with controls, each group of patients showed a widespread pattern of WM damage involving anterior and posterior regions (Fig. A.1). Compared with bvFTD patients, EOAD showed higher axD of the splenium of the CC and the right posterior cingulum (Fig. 2). Compared with EOAD, bvFTD patients showed decreased FA and increased radD of the whole CC (mainly the genu), SLF, ILF and uncinate fasciculi bilaterally, internal and external capsule bilaterally, and left anterior cingulum (Fig. 2); increased MD of the genu of CC, ILF and uncinate fasciculi bilaterally, and internal and external capsule bilaterally (Fig. 2); and increased axD of the genu of CC, right uncinate fasciculus, and WM underneath the right lateral orbitofrontal cortex.

3.4. WM microstructure: Tractography

Compared with healthy controls, bvFTD and EOAD patients showed a widespread pattern of WM damage involving all investigated tracts (Table A.3). Compared to EOAD, bvFTD patients showed greater WM damage of the genu of CC, uncinate fasciculus bilaterally, and left SLF (Table A.3; Fig. 2).

3.5. Resting state functional connectivity

Within the DMN, EOAD patients showed reduced functional connectivity of the precunes bilaterally and the right calcarine cortex compared with controls, and the calcarine cortex bilaterally, left posterior cingulate cortex, left precuneus and right cuneus compared with bvFTD patients (Table A.4; Fig. A.2). No between-group differences were observed in the other RS networks of interest.

3.6. Correlation analysis

In EOAD patients, positive relationships were observed between executive Z score and fronto-parietal cortical thickness measures, and between memory Z score and the parieto-temporal cortical thickness measures (Table A.5). No other significant correlations were found.

3.7. Discrimination analysis

Fig. 3 shows the results of the random forest analysis for cortical thickness and tractography measures, separately (for each MR modality, the first five MRI variables in terms of importance in classifying diagnosis are provided). Among cortical thickness measures, the highest discrimination ability in distinguishing EOAD and bvFTD patients was achieved by the cortical thickness of the left inferior parietal gyrus, followed by the right temporal pole, left isthmus of cingulum, right inferior parietal gyrus and right precuneus (Fig. 3). When taken together, all these cortical thickness measures were able to distinguish patients with EOAD from bvFTD with high accuracy, specificity, and sensitivity (Table 2). Among WM tractography measures, the highest discrimination ability in distinguishing the two patient groups was obtained by the right uncinate fasciculus axD, followed by the radD, MD and FA values of the same WM tract, and the genu of the CC FA (Fig. 3). When taken together, all these WM tractography measures were able to distinguish patients with EOAD from bvFTD with high

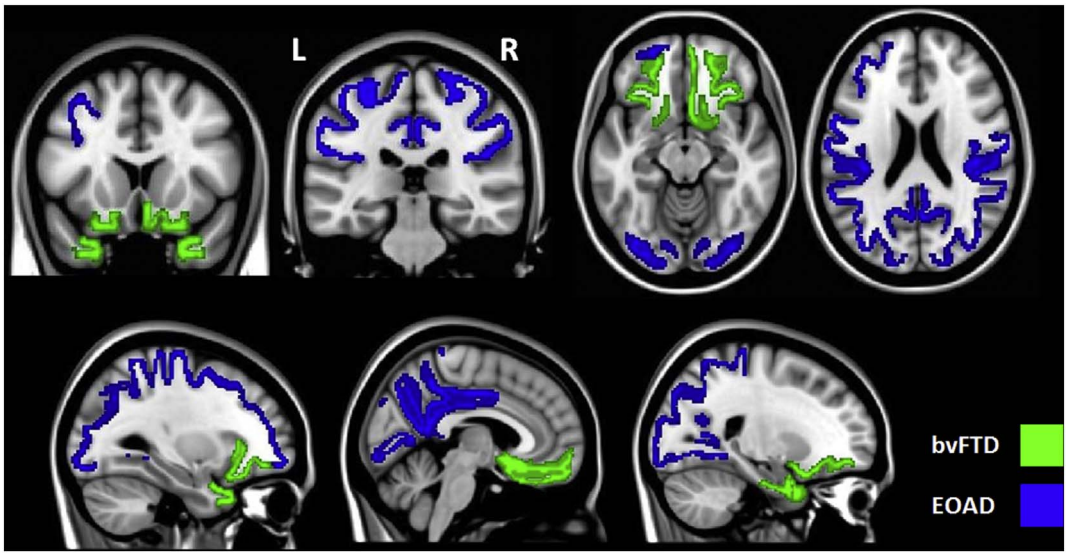

Fig. 1. Cortical thickness findings. Patterns of regional cortical thinning of early onset Alzheimer's disease (EOAD) patients compared to cases with the behavioural variant of frontotemporal dementia (bvFTD) (blue) and *vice versa* (green). Results are overlaid on the Montreal Neurological Institute standard brain and shown at $p < 0.05$ False Discovery Rate-corrected for multiple comparisons. R = right; L = left.

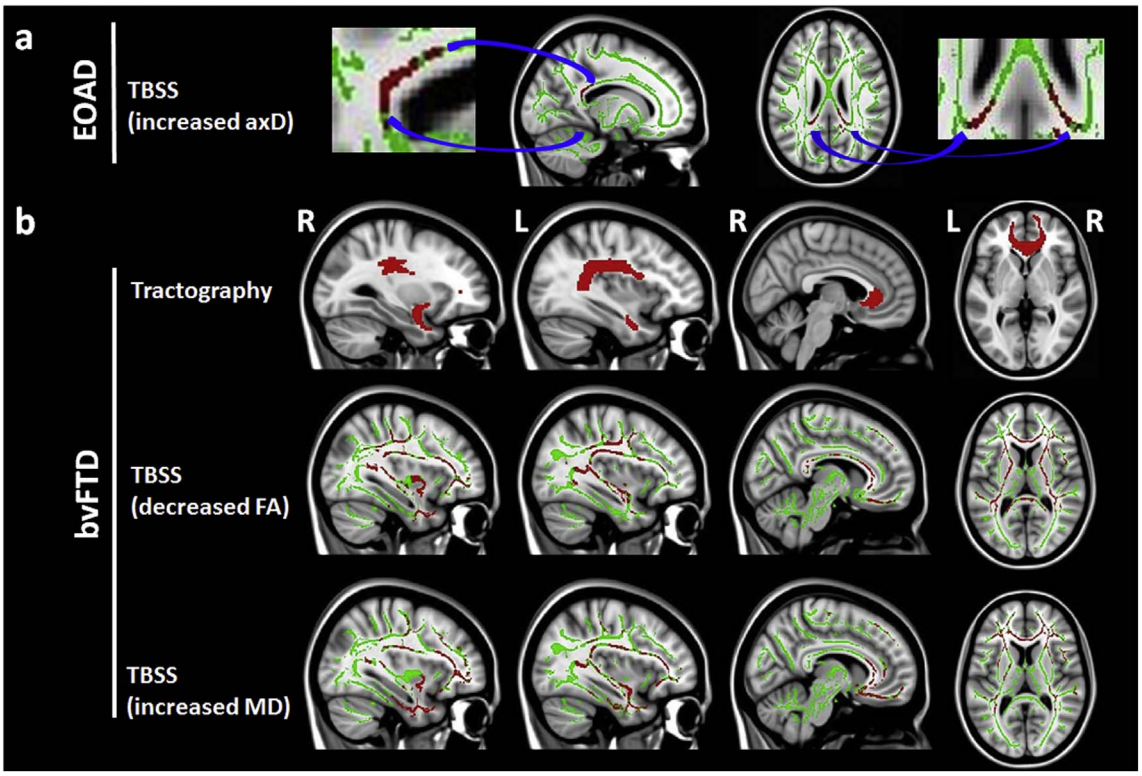

Fig. 2. Diffusion tensor MRI findings. A) Tract-Based Spatial Statistics (TBSS) results in early onset Alzheimer's disease (EOAD) patients compared to cases with the behavioural variant of frontotemporal dementia (bvFTD). The significant voxels are magnified for a better view. B) Tractography and TBSS findings in bvFTD patients relative to EOAD cases. TBSS results are shown in red (fractional anisotropy [FA], mean diffusivity [MD] and axial diffusivity [axD]) on the white matter (WM) skeleton (light green) and displayed on the sagittal and axial sections of the Montreal Neurological Institute (MNI) standard brain in neurological convention ($p < 0.05$ corrected for multiple comparisons at the cluster level using the threshold-free cluster enhancement option). WM tracts showing altered diffusion tensor MRI values are shown in red on the MNI standard brain in neurological convention ($p < 0.05$, false discovery rate-corrected for multiple comparisons). R = right; L = left.

accuracy and specificity, but low sensitivity (Table 2). A model combining the five best cortical thickness measures and the five best DT MRI measures was able to distinguish patients with EOAD and bvFTD with high accuracy, specificity, and the highest sensitivity (Table 2). When all the best MRI variables entered a random forest analysis, the highest discrimination ability was achieved by the cortical thickness of the left inferior parietal gyrus (Normalized Variable Importance [NVI] = 100.0), followed by the right temporal pole (NVI = 82.5), right precuneus (NVI = 75.8), left isthmus of cingulum (NVI = 60.9), and left superior parietal gyrus (NVI = 60.9).

3.8. Analysis of a sub-sample of patients with CSF and/or PET diagnostic biomarkers

The patterns of voxel-wise WM damage and resting state functional connectivity well overlapped with those obtained in the entire sample through all comparisons. Compared to bvFTD cases, EOAD patients showed further cortical thinning of the left middle and transverse temporal gyri, left cuneus and precentral gyri. In addition to the results obtained in the entire sample, tractography analysis showed increased axD of the splenium of CC in EOAD relative to bvFTD and increased MD of the genu of CC in the opposite comparison. Random forest analysis in this sub-sample took into account these additional significant variables. The random forest results together with the diagnostic performance of the best MRI classification variables are shown in Table 2 in comparison to the data of the entire sample (Table 2). In patients with a biomarker-based diagnosis, specificity and sensitivity of the classification provided by the WM measures increased as well as accuracy and specificity of the combined model (5 cortical thickness + 5 WM best measures; Table 2).

4. Discussion

This multiparametric study builds upon and extends previous studies of MRI patterns to distinguish *in vivo* EOAD and bvFTD patients. The major strengths of our report compared with previous literature are the combination of different MRI modalities to explore the GM and WM damage in these patients, and the application of the random forest analysis (Breiman, 2001) to select the most probable MRI *in vivo* predictors of EOAD and bvFTD at an individual patient level.

When compared with controls, both groups of patients showed a severe impairment in all cognitive domains and a similar pattern of brain alterations involving anterior and posterior regions. The direct comparison between patient groups provided syndrome-specific patterns of damage. Compared with bvFTD, EOAD patients showed a prominent cortical damage of parietal and occipital lobes and decreased functional connectivity of the parieto-occipital cortex within the DMN. Compared with EOAD, bvFTD patients showed cortical alterations of orbitofrontal cortex and temporal pole, and a severe pattern of WM damage involving anterior but also posterior WM tracts. The random forest analysis suggested that the left inferior parietal cortical thickness measure and the WM integrity of the right uncinate fasciculus (most affected in EOAD and in bvFTD cases, respectively) were the best predictors of clinical diagnosis. Finally, a model combining the best GM and WM predictors provided high accuracy (0.82) and specificity (0.76), and the highest sensitivity (0.96).

Although EOAD showed a widespread pattern of cognitive and brain alterations, the parietal lobe remains the most affected region relative to bvFTD. Previous studies demonstrated the severe involvement of parietal regions in EOAD investigating cortical and WM damage (Canu et al., 2013; Canu et al., 2012; Frisoni et al., 2007), amyloid deposits and glucose hypometabolism (Ossenkoppele et al., 2012). This region is

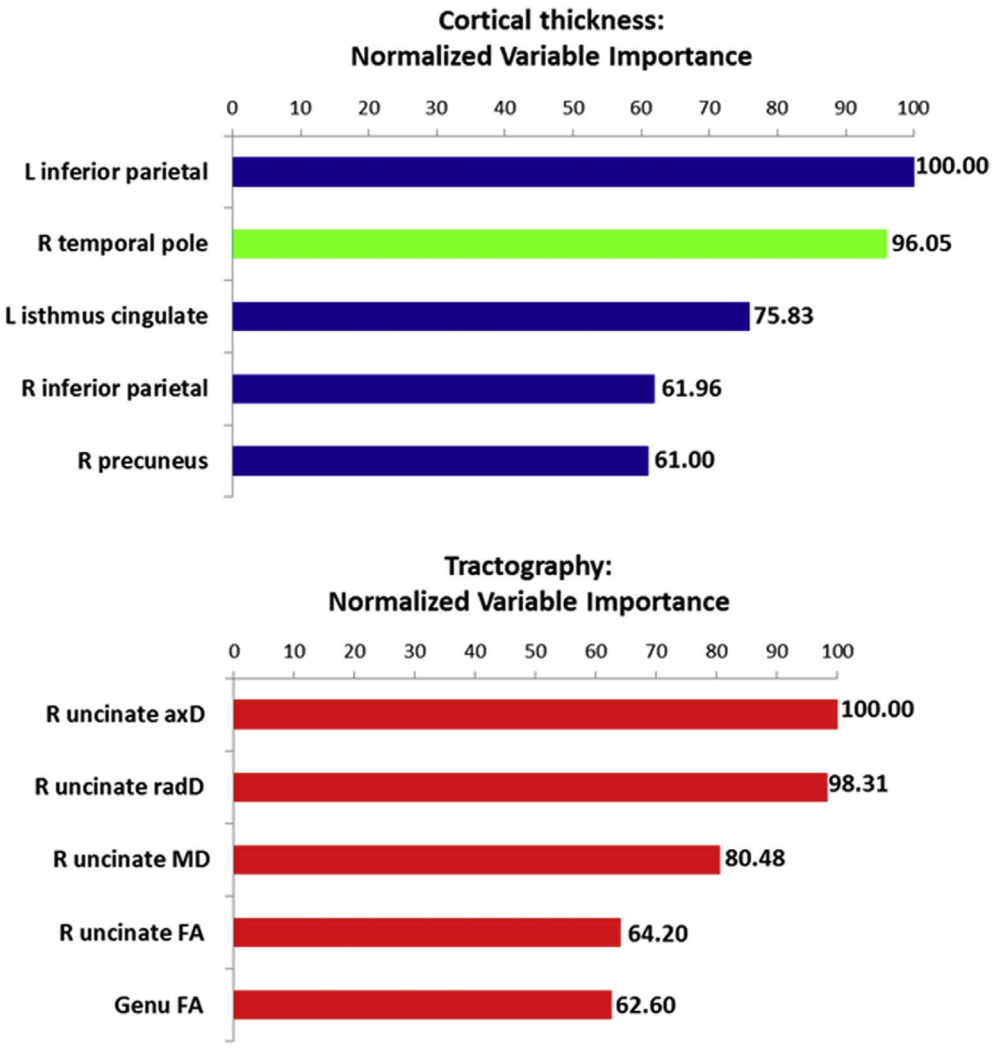

Fig. 3. Random forest analysis. Normalized variable importance of the five best MRI variables in distinguishing patients with early onset Alzheimer's disease (EOAD) and the behavioural variant of frontotemporal dementia (bvFTD), among A) cortical thickness measures (blue: greater cortical thinning in EOAD relative to bvFTD; green: greater cortical thinning in bvFTD relative to EOAD) and B) tractography measures (red; all regions showed greater damage in bvFTD compared to EOAD).

Table 2
Random Forrest and diagnostic performance of the best MRI variables in distinguishing EOAD and bvFTD patients.

Total sample					Sub-sample with biomarker-based diagnosis				
Model	RF				Model	RF			
CT	NVI	Accuracy	Specificity	Sensitivity	CT	NVI	Accuracy	Specificity	Sensitivity
L inferior parietal	100	0.78	0.76	0.83	L inferior parietal	100	0.66	0.72	0.64
R temporal pole	96.05	–	–	–	R precuneus	57.2	–	–	–
L isthmus cingulate	75.83	–	–	–	L isthmus cingulate	51.4	–	–	–
R inferior parietal	61.96	–	–	–	R inferior parietal	18.7	–	–	–
R precuneus	61.00	–	–	–	R superior parietal	11.0	–	–	–
All 5 CT measures	–	0.82	0.80	0.87	All 5 CT measures	–	0.83	0.83	0.80
WM tracts					WM tracts				
R uncinate, axD	100	0.81	0.96	0.43	R uncinate, radD	100	0.72	0.74	0.67
R uncinate, radD	98.31	–	–	–	L uncinate, axD	84	–	–	–
R uncinate, MD	80.48	–	–	–	R uncinate, MD	64.6	–	–	–
R uncinate, FA	64.20	–	–	–	R uncinate, FA	26.8	–	–	–
Genu of CC, FA	62.60	–	–	–	R uncinate, axD	7.6	–	–	–
All 5 WM tract measures	–	0.81	0.89	0.61	All 5 WM tract measures	–	0.89	0.92	0.81
All 5 CT + 5 WM tract measures	–	0.82	0.76	0.96	All 5 CT + 5 WM tract measures	–	0.97	0.90	0.95
CT + WM tracts					CT + WM tracts				
L inferior parietal	100	0.78	0.76	0.83	L inferior parietal	100	0.66	0.72	0.64
R temporal pole	82.5	–	–	–	R precuneus	63.0	–	–	–
R precuneus	75.8	–	–	–	L isthmus cingulate	61.4	–	–	–
L isthmus cingulate	60.9	–	–	–	R inferior parietal	26.7	–	–	–
L superior parietal	60.9	–	–	–	R superior parietal	22.4	–	–	–
All 5 measures	–	0.84	0.79	0.81	All 5 measures	–	0.83	0.83	0.80

Abbreviations: axD = axial diffusivity; AUC = area under the curve; CC = corpus callosum; CT = cortical thickness; FA = fractional anisotropy; L = left; MD = mean diffusivity; NVI: Normalized Variable Importance; R = Right; radD: radial diffusivity; RF = Random Forest; WM = white matter.

implicated in several cognitive domains involved in this condition, such as episodic memory retrieval, spatial and visual construction and in executive functions associated with the parietal projections to the frontal lobes (Gottlieb, 2007). On the contrary, the right temporal pole atrophy, which was more severe in bvFTD patients, well reflects their greater pattern of behavioural disturbances compared to EOAD. In fact, right temporal pole atrophy has been related to changes in personality and socially appropriate behavior, lack of empathy and eating compulsive behavior (Gorno-Tempini et al., 2004). The few existing studies comparing GM atrophy patterns between AD and bvFTD patients showed precuneus and lateral parietal cortices to be more atrophic in AD, and temporal pole and anterior cingulate more severely damaged in bvFTD (Du et al., 2007; Rabinovici et al., 2007). It is noteworthy that the thinning of the medial temporal gyri (MTL) was not able to distinguish the two clinical syndromes since it was present in both groups relative to healthy controls. This finding sustains previous evidence that measures of MTL are good markers to differentiate AD from normals (Dubois et al., 2014; McKhann et al., 2011) but are less effective in differentiating AD from bvFTD (de Souza et al., 2013) .

In keeping with previous studies (Kuceyeski et al., 2012; McMillan et al., 2012; Moller et al., 2015), frontal WM tract damage was the most accurate WM measure to differentiate bvFTD from AD cases and axD was the best DT MRI metric to support differential diagnosis (Moller et al., 2015). Specifically, in bvFTD we observed that DT MRI measures of the uncinate fasciculus and genu of the CC were the best WM predictors of the clinical diagnosis relative to EOAD cases. The greater WM involvement in bvFTD compared to AD has been previously suggested by neuroimaging studies (Lu et al., 2014; Mahoney et al., 2014; McMillan et al., 2012; Moller et al., 2015; Zhang et al., 2011; Zhang et al., 2009). Taken together with previous findings, our results demonstrated that bvFTD patients have significantly greater WM breakdown in late-myelinating regions reaching the frontal lobe relative to EOAD. Notably, the CC is involved in both patient groups when compared with controls; however, the damage was clearly more prominent in the genu in the bvFTD group and in the splenium in the EOAD group. This finding supports previous atrophy (Walterfang et al., 2014; Yamauchi et al., 2000) and DT MRI studies (Lu et al., 2014; Mahoney et al., 2014; McMillan et al., 2012; Moller et al., 2015; Zhang et al., 2011; Zhang et al., 2009) suggesting that the regional pattern of callosal damage may distinguish the two neurodegenerative dementia.

DT MRI findings suggest that WM degeneration is more prominent in bvFTD than in AD. Although caution is needed since we do not have pathological-proven diagnosis, different underlying pathology (amyloid, tau, TDP-43) might be responsible for these changes. The greater WM alterations might reflect abundant tau/TDP pathology in glial cells and altered axonal transport in frontotemporal lobar degeneration (FTLD) cases which may ultimately result in axonal degeneration (Agosta et al., 2015; Brettschneider et al., 2014; Brettschneider et al., 2013; Forman et al., 2002; Neumann et al., 2007; Zhukareva et al., 2006). The greater spatial extent of WM damage in FTLD might also reflect distal propagation of pathology from primarily involved regions adjacent to GM damage, due for example to pathogeneic protein diffusion (Hardy and Revesz, 2012). The burden of WM degeneration has also been suggested to be different depending on underlying FTLD pathology, being greater in tau relative to TDP-43 cases (McMillan et al., 2013). Several neuroimaging studies reported a more severe WM involvement in FTLD-tau relative to FTLD-TDP cases using atrophy (Caso et al., 2013; Kim et al., 2007; Spinelli et al., 2017) or DT MRI measures (Agosta et al., 2015; McMillan et al., 2013; Sajjadi et al., 2013). The lack of pathological diagnosis did not allow us to explore the patterns of WM damage in relation to FTLD pathology.

When CSF and FDG PET biomarkers were used to support the clinical diagnosis of EAOD and bvFTD, both specificity and sensitivity increased in the WM model and, likely driven by WM findings, the combined cortical and WM model was the most powerful in terms of accuracy. These findings obtained in patients with a higher diagnostic certainty (McKhann et al., 2011; Rascovsky et al., 2011) support the robustness of our results and their applicability in clinical samples.

EOAD patients showed a reduced functional connectivity in the parietal cortex within the DMN compared to both healthy controls and bvFTD, as previously shown in classical LOAD cases (Zhou et al., 2010). These findings suggest that, regardless the age at disease onset, the reduced functional connectivity in the parietal regions remains a peculiar feature of AD. Compared to LOAD, EOAD patients showed further functional abnormalities in the occipital regions likely reflecting the greater amount of their visuospatial deficits (Snowden et al., 2007). In our EOAD sample, we did not observe altered connectivity in non-DMN networks as suggested by recent studies (Lehmann et al., 2015). A possible explanation of this latter finding is that our EOAD patients had a shorter disease duration (3.6 ± 1.3 years) relative to those of the previous study (5.8 ± 3.5 years) (Lehmann et al., 2015). Furthermore, unexpectedly, in bvFTD we did not observe a reduced functional connectivity of the anterior regions in the salience network (Filippi et al., 2013; Zhou et al., 2010). This discrepancy is unlikely due to the sample clinical features (in all studies, bvFTD cases were similar), but it could be attributed to the 1.5 T MR scanner used in the present work compared with the 3.0 T machines employed in previous studies (Filippi et al., 2013; Zhou et al., 2010). While taking full account of these caveats, the lack of functional connectivity changes in bvFTD patients showing severe WM microstructural alterations may suggest that a reduced structural integrity precedes functional alterations (Schmidt et al., 2014). However, only longitudinal investigations in larger patient populations can clarify the temporal relationship between structural and functional changes.

When MRI measures were combined, the discrimination analysis showed that GM variables were the best predictors of clinical diagnosis. Previous literature is not consistent in this regard. Some studies that used MRI-based classification models (McMillan et al., 2012; Moller et al., 2015) observed that an approach combining GM and WM measures is the best for the correct classification of patients. On the contrary, one study observed that WM measures (obtained by averaging each DT metric across all the injured WM connections among 116 tract pairs) are the best to correctly classify the patients (Kuceyeski et al., 2012). The discrepancy between previous (Kuceyeski et al., 2012; McMillan et al., 2012; Moller et al., 2015) and our study could be due to different clinical populations (in previous studies not all AD patients were EOAD, and/or bvFTD cases were included in a larger, clinically heterogeneous FTD group) (Kuceyeski et al., 2012; McMillan et al., 2012; Moller et al., 2015), MRI scanners, type of analyses (*e.g.*, volumetric *vs* cortical thickness), and statistical approach. Our study suggests that when homogeneous populations of bvFTD and EOAD patients in their mild to moderate phase of the disease are studied, GM measures outperformed in providing classification relative to other MRI modalities.

Some methodological shortcomings should be considered when interpreting our data.

An important caveat is that the gold standard in our study was the clinical diagnosis since no pathological confirmation of diagnosis. However, all patients underwent an extensive dementia screening and were evaluated in a multidisciplinary panel including clinicians specialized in dementia. In addition, the clinical diagnosis was biomarker-based according to diagnostic criteria (McKhann et al., 2011; Rascovsky et al., 2011) in > 80% of patients, thus increasing diagnostic certainty. Also, lack of postmortem evaluation did not allow us to investigate the different patterns of brain damage in bvFTD patients according to the underlying FTLD-tau or FTLD-TDP pathology. Second, we did not include patients with atypical AD such as the frontal variant. Third, unlike MRI, *in vivo* imaging with radioligand PET can provide disease-specific markers of neurodegeneration (Villemagne et al., 2017). However, 30% of healthy elderly subjects have significant levels of cortical amyloid deposition (Rowe et al., 2010); the value of tau imaging in differentiating distinct tauopathies as well as the specificity of

binding to tau remain largely unresolved; and, to date, radioligands to measure TDP-43 are not yet available. In this context, advanced MRI techniques can contribute to the noninvasive assessment of dementia. Clearly, more effort should be made to provide cut-off values to be applied in single patients, which would allow MRI-based models to be better included in clinical neuroimaging/clinical practice.

5. Conclusions

In conclusion, a multiparametric MRI study is useful to identify brain alterations which are specific to EOAD and bvFTD. A severe cortical involvement is suggestive of EOAD while a prominent WM damage might be indicative of bvFTD. Future studies, including larger clinical populations recruited in the early stage and using harmonized protocols are warranted to confirm the diagnostic contribution of advanced MRI techniques in neurodegenerative dementia.

Supplementary data to this article can be found online at http://dx.doi.org/10.1016/j.nicl.2017.05.018.

Funding

This study was partially supported by a grant from the Ministry of Education and Science, Republic of Serbia (project 175090).

Disclosure statement

E. Canu has received research support from the Italian Ministry of Health.

F. Agosta is Section Editor of *NeuroImage: Clinical*; has received speaker honoraria from EXCEMED– Excellence in Medical Education; and receives research supports from the Italian Ministry of Health, AriSLA (Fondazione Italiana di Ricerca per la SLA), and the European Research Council.

G. Mandic-Stojmenovic, T. Stojković, E. Stefanova, and F. Imperiale report no disclosures.

A. Inuggi has received research supports from AriSLA (Fondazione Italiana di Ricerca per la SLA).

M. Copetti has received compensation for consulting and/or serving on advisory boards from Teva Pharmaceuticals and Biogen Idec.

V. Kostic has received research grants from Ministry of Education and Science, Republic of Serbia and the Serbian Academy of Science and Arts; he receives research supports from Valeant, Stada, Novartis and Boehriner Ingelheim, and speaker honoraria from Novartis and Boehringer Ingelheim.

M. Filippi is Editor-in-Chief of *Journal of Neurology*; serves on scientific advisory board for Teva Pharmaceutical Industries; has received compensation for consulting services and/or speaking activities from Bayer Schering Pharma, Biogen Idec, EXCEMED, Merck Serono, and Teva Pharmaceutical Industries; and receives research support from Bayer Schering Pharma, Biogen Idec, Merck Serono, Teva Pharmaceutical Industries, Italian Ministry of Health, Fondazione Italiana Sclerosi Multipla, Cure PSP, Alzheimer's and Drug Discovery Foundation, and the Jacques and Gloria Gossweiler Foundation (Switzerland).

References

Agosta, F., Galantucci, S., Magnani, G., Marcone, A., Martinelli, D., Antonietta Volonte, M., Riva, N., Iannaccone, S., Ferraro, P.M., Caso, F., Chio, A., Comi, G., Falini, A., Filippi, M., 2015. MRI signatures of the frontotemporal lobar degeneration continuum. Hum. Brain Mapp. 36, 2602–2614.

Alladi, S., Xuereb, J., Bak, T., Nestor, P., Knibb, J., Patterson, K., Hodges, J.R., 2007. Focal cortical presentations of Alzheimer's disease. Brain 130, 2636–2645.

Andersson, J.L., Jenkinson, M., Smith, S., 2007. Non-linear registration, aka spatial normalisation. In: Technical Report. FMRIB Centre, Oxford, United Kingdom.

Beckmann, C.F., DeLuca, M., Devlin, J.T., Smith, S.M., 2005. Investigations into resting-state connectivity using independent component analysis. Philos. Trans. R. Soc. Lond. Ser. B Biol. Sci. 360, 1001–1013.

Behrens, T.E., Berg, H.J., Jbabdi, S., Rushworth, M.F., Woolrich, M.W., 2007. Probabilistic diffusion tractography with multiple fibre orientations: what can we gain? NeuroImage 34, 144–155.

Benton, A., 1968. Differential behavioural effects in frontal lobe disease. Neuropsychologia 6, 53–60.

Breiman, L., 2001. Random forests. Mach. Learn. 45, 5–32.

Brettschneider, J., Del Tredici, K., Toledo, J.B., Robinson, J.L., Irwin, D.J., Grossman, M., Suh, E., Van Deerlin, V.M., Wood, E.M., Baek, Y., Kwong, L., Lee, E.B., Elman, L., McCluskey, L., Fang, L., Feldengut, S., Ludolph, A.C., Lee, V.M., Braak, H., Trojanowski, J.Q., 2013. Stages of pTDP-43 pathology in amyotrophic lateral sclerosis. Ann. Neurol. 74, 20–38.

Brettschneider, J., Del Tredici, K., Irwin, D.J., Grossman, M., Robinson, J.L., Toledo, J.B., Fang, L., Van Deerlin, V.M., Ludolph, A.C., Lee, V.M., Braak, H., Trojanowski, J.Q., 2014. Sequential distribution of pTDP-43 pathology in behavioral variant frontotemporal dementia (bvFTD). Acta Neuropathol. 127, 423–439.

Canu, E., Frisoni, G.B., Agosta, F., Pievani, M., Bonetti, M., Filippi, M., 2012. Early and late onset Alzheimer's disease patients have distinct patterns of white matter damage. Neurobiol. Aging 33, 1023–1033.

Canu, E., Agosta, F., Spinelli, E.G., Magnani, G., Marcone, A., Scola, E., Falautano, M., Comi, G., Falini, A., Filippi, M., 2013. White matter microstructural damage in Alzheimer's disease at different ages of onset. Neurobiol. Aging 34, 2331–2340.

Canu, E., Kostic, M., Agosta, F., Munjiza, A., Ferraro, P.M., Pesic, D., Copetti, M., Peljto, A., Tosevski, D.L., Filippi, M., 2015. Brain structural abnormalities in patients with major depression with or without generalized anxiety disorder comorbidity. J. Neurol. 262, 1255–1265.

Caso, F., Gesierich, B., Henry, M., Sidhu, M., LaMarre, A., Babiak, M., Miller, B.L., Rabinovici, G.D., Huang, E.J., Magnani, G., Filippi, M., Comi, G., Seeley, W.W., Gorno-Tempini, M.L., 2013. Nonfluent/agrammatic PPA with *in-vivo* cortical amyloidosis and Pick's disease pathology. Behav. Neurol. 26, 95–106.

Cooper, J.A., Sagar, H.J., Jordan, N., Harvey, N.S., Sullivan, E.V., 1991. Cognitive impairment in early, untreated Parkinson's disease and its relationship to motor disability. Brain 114 (Pt. 5), 2095–2122.

Cummings, J.L., Mega, M., Gray, K., Rosenberg-Thompson, S., Carusi, D.A., Gornbein, J., 1994. The neuropsychiatric Inventory: comprehensive assessment of psychopathology in dementia. Neurology 44, 2308–2314.

Dale, A.M., Fischl, B., Sereno, M.I., 1999. Cortical surface-based analysis I. Segmentation and surface reconstruction. NeuroImage 9, 179–194.

Dani, M., Brooks, D.J., Edison, P., 2016. Tau imaging in neurodegenerative diseases. Eur. J. Nucl. Med. Mol. Imaging 43, 1139–1150.

Desikan, R.S., Segonne, F., Fischl, B., Quinn, B.T., Dickerson, B.C., Blacker, D., Buckner, R.L., Dale, A.M., Maguire, R.P., Hyman, B.T., Albert, M.S., Killiany, R.J., 2006. An automated labeling system for subdividing the human cerebral cortex on MRI scans into gyral based regions of interest. NeuroImage 31, 968–980.

Du, A.T., Schuff, N., Kramer, J.H., Rosen, H.J., Gorno-Tempini, M.L., Rankin, K., Miller, B.L., Weiner, M.W., 2007. Different regional patterns of cortical thinning in Alzheimer's disease and frontotemporal dementia. Brain 130, 1159–1166.

Dubois, B., Slachevsky, A., Litvan, I., Pillon, B., 2000. The FAB: a frontal assessment battery at bedside. Neurology 55, 1621–1626.

Dubois, B., Feldman, H.H., Jacova, C., Hampel, H., Molinuevo, J.L., Blennow, K., DeKosky, S.T., Gauthier, S., Selkoe, D., Bateman, R., Cappa, S., Crutch, S., Engelborghs, S., Frisoni, G.B., Fox, N.C., Galasko, D., Habert, M.O., Jicha, G.A., Nordberg, A., Pasquier, F., Rabinovici, G., Robert, P., Rowe, C., Salloway, S., Sarazin, M., Epelbaum, S., de Souza, L.C., Vellas, B., Visser, P.J., Schneider, L., Stern, Y., Scheltens, P., Cummings, J.L., 2014. Advancing research diagnostic criteria for Alzheimer's disease: the IWG-2 criteria. Lancet Neurol. 13, 614–629.

Efron, B., Tibshirani, R.J., 1997. Improvements on cross-validation: the .632 + bootstrap method. J. Am. Stat. Assoc. 92, 548–560.

Filippi, M., Agosta, F., Scola, E., Canu, E., Magnani, G., Marcone, A., Valsasina, P., Caso, F., Copetti, M., Comi, G., Cappa, S.F., Falini, A., 2013. Functional network connectivity in the behavioral variant of frontotemporal dementia. Cortex 49, 2389–2401.

Filippini, N., MacIntosh, B.J., Hough, M.G., Goodwin, G.M., Frisoni, G.B., Smith, S.M., Matthews, P.M., Beckmann, C.F., Mackay, C.E., 2009. Distinct patterns of brain activity in young carriers of the APOE-epsilon4 allele. Proc. Natl. Acad. Sci. U. S. A. 106, 7209–7214.

Fischl, B., Dale, A.M., 2000. Measuring the thickness of the human cerebral cortex from magnetic resonance images. Proc. Natl. Acad. Sci. U. S. A. 97, 11050–11055.

Folstein, M.F., Folstein, S.E., McHugh, P.R., 1975. "Mini-mental state". A practical method for grading the cognitive state of patients for the clinician. J. Psychiatr. Res. 12, 189–198.

Forman, M.S., Zhukareva, V., Bergeron, C., Chin, S.S., Grossman, M., Clark, C., Lee, V.M., Trojanowski, J.Q., 2002. Signature tau neuropathology in gray and white matter of corticobasal degeneration. Am. J. Pathol. 160, 2045–2053.

Frisoni, G.B., Pievani, M., Testa, C., Sabattoli, F., Bresciani, L., Bonetti, M., Beltramello, A., Hayashi, K.M., Toga, A.W., Thompson, P.M., 2007. The topography of grey matter involvement in early and late onset Alzheimer's disease. Brain 130, 720–730.

Gorno-Tempini, M.L., Rankin, K.P., Woolley, J.D., Rosen, H.J., Phengrasamy, L., Miller, B.L., 2004. Cognitive and behavioral profile in a case of right anterior temporal lobe neurodegeneration. Cortex 40, 631–644.

Gottlieb, J., 2007. From thought to action: the parietal cortex as a bridge between perception, action, and cognition. Neuron 53, 9–16.

Greve, D.N., Fischl, B., 2009. Accurate and robust brain image alignment using boundary-based registration. NeuroImage 48, 63–72.

Grober, E., Buschke, H., 1987. Genuine memory deficits in dementia. Dev. Neuropsychol. 3, 13–36.

Hardy, J., Revesz, T., 2012. The spread of neurodegenerative disease. N. Engl. J. Med.

366, 2126–2128.
Harris, J.M., Gall, C., Thompson, J.C., Richardson, A.M., Neary, D., du Plessis, D., Pal, P., Mann, D.M., Snowden, J.S., Jones, M., 2013. Sensitivity and specificity of FTDC criteria for behavioral variant frontotemporal dementia. Neurology 80, 1881–1887.
Jack Jr., C.R., Bennett, D.A., Blennow, K., Carrillo, M.C., Feldman, H.H., Frisoni, G.B., Hampel, H., Jagust, W.J., Johnson, K.A., Knopman, D.S., Petersen, R.C., Scheltens, P., Sperling, R.A., Dubois, B., 2016. A/T/N: An unbiased descriptive classification scheme for Alzheimer disease biomarkers. Neurology 87, 539–547.
Jenkinson, M., Smith, S., 2001. A global optimisation method for robust affine registration of brain images. Med. Image Anal. 5, 143–156.
Jenkinson, M., Beckmann, C.F., Behrens, T.E., Woolrich, M.W., Smith, S.M., 2012. Fsl. NeuroImage 62, 782–790.
Johnson, J.K., Head, E., Kim, R., Starr, A., Cotman, C.W., 1999. Clinical and pathological evidence for a frontal variant of Alzheimer disease. Arch. Neurol. 56, 1233–1239.
Kim, E.J., Rabinovici, G.D., Seeley, W.W., Halabi, C., Shu, H., Weiner, M.W., DeArmond, S.J., Trojanowski, J.Q., Gorno-Tempini, M.L., Miller, B.L., Rosen, H.J., 2007. Patterns of MRI atrophy in tau positive and ubiquitin positive frontotemporal lobar degeneration. J. Neurol. Neurosurg. Psychiatry 78, 1375–1378.
Kuceyeski, A., Zhang, Y., Raj, A., 2012. Linking white matter integrity loss to associated cortical regions using structural connectivity information in Alzheimer's disease and fronto-temporal dementia: the loss in connectivity (LoCo) score. NeuroImage 61, 1311–1323.
Lehmann, M., Madison, C., Ghosh, P.M., Miller, Z.A., Greicius, M.D., Kramer, J.H., Coppola, G., Miller, B.L., Jagust, W.J., Gorno-Tempini, M.L., Seeley, W.W., Rabinovici, G.D., 2015. Loss of functional connectivity is greater outside the default mode network in nonfamilial early-onset Alzheimer's disease variants. Neurobiol. Aging 36, 2678–2686.
Lu, P.H., Lee, G.J., Shapira, J., Jimenez, E., Mather, M.J., Thompson, P.M., Bartzokis, G., Mendez, M.F., 2014. Regional differences in white matter breakdown between frontotemporal dementia and early-onset Alzheimer's disease. J. Alzheimers Dis. 39, 261–269.
Mahoney, C.J., Ridgway, G.R., Malone, I.B., Downey, L.E., Beck, J., Kinnunen, K.M., Schmitz, N., Golden, H.L., Rohrer, J.D., Schott, J.M., Rossor, M.N., Ourselin, S., Mead, S., Fox, N.C., Warren, J.D., 2014. Profiles of white matter tract pathology in frontotemporal dementia. Hum. Brain Mapp. 35, 4163–4179.
McKhann, G.M., Knopman, D.S., Chertkow, H., Hyman, B.T., Jack Jr., C.R., Kawas, C.H., Klunk, W.E., Koroshetz, W.J., Manly, J.J., Mayeux, R., Mohs, R.C., Morris, J.C., Rossor, M.N., Scheltens, P., Carrillo, M.C., Thies, B., Weintraub, S., Phelps, C.H., 2011. The diagnosis of dementia due to Alzheimer's disease: recommendations from the National Institute on Aging-Alzheimer's Association workgroups on diagnostic guidelines for Alzheimer's disease. Alzheimers Dement. 7, 263–269.
McMillan, C.T., Brun, C., Siddiqui, S., Churgin, M., Libon, D., Yushkevich, P., Zhang, H., Boller, A., Gee, J., Grossman, M., 2012. White matter imaging contributes to the multimodal diagnosis of frontotemporal lobar degeneration. Neurology 78, 1761–1768.
McMillan, C.T., Irwin, D.J., Avants, B.B., Powers, J., Cook, P.A., Toledo, J.B., McCarty Wood, E., Van Deerlin, V.M., Lee, V.M., Trojanowski, J.Q., Grossman, M., 2013. White matter imaging helps dissociate tau from TDP-43 in frontotemporal lobar degeneration. J. Neurol. Neurosurg. Psychiatry 84, 949–955.
Mendez, M.F., Joshi, A., Tassniyom, K., Teng, E., Shapira, J.S., 2013. Clinicopathologic differences among patients with behavioral variant frontotemporal dementia. Neurology 80, 561–568.
Mioshi, E., Dawson, K., Mitchell, J., Arnold, R., Hodges, J.R., 2006. The Addenbrooke's cognitive examination revised (ACE-R): a brief cognitive test battery for dementia screening. Int. J. Geriatr. Psychiatry 21, 1078–1085.
Moller, C., Hafkemeijer, A., Pijnenburg, Y.A., Rombouts, S.A., van der Grond, J., Dopper, E., van Swieten, J., Versteeg, A., Pouwels, P.J., Barkhof, F., Scheltens, P., Vrenken, H., van der Flier, W.M., 2015. Joint assessment of white matter integrity, cortical and subcortical atrophy to distinguish AD from behavioral variant FTD: a two-center study. Neuroimage Clin. 9, 418–429.
Neumann, M., Kwong, L.K., Truax, A.C., Vanmassenhove, B., Kretzschmar, H.A., Van Deerlin, V.M., Clark, C.M., Grossman, M., Miller, B.L., Trojanowski, J.Q., Lee, V.M., 2007. TDP-43-positive white matter pathology in frontotemporal lobar degeneration with ubiquitin-positive inclusions. J. Neuropathol. Exp. Neurol. 66, 177–183.
Ossenkoppele, R., Zwan, M.D., Tolboom, N., van Assema, D.M., Adriaanse, S.F., Kloet, R.W., Boellaard, R., Windhorst, A.D., Barkhof, F., Lammertsma, A.A., Scheltens, P., van der Flier, W.M., van Berckel, B.N., 2012. Amyloid burden and metabolic function in early-onset Alzheimer's disease: parietal lobe involvement. Brain 135, 2115–2125.
Passamonti, L., Vazquez Rodriguez, P., Hong, Y.T., Allinson, K.S., Williamson, D., Borchert, R.J., Sami, S., Cope, T.E., Bevan-Jones, W.R., Jones, P.S., Arnold, R., Surendranathan, A., Mak, E., Su, L., Fryer, T.D., Aigbirhio, F.I., O'Brien, J.T., Rowe, J.B., 2017. 18F-AV-1451 positron emission tomography in Alzheimer's disease and progressive supranuclear palsy. Brain 140, 781–791.
Picard, C., Pasquier, F., Martinaud, O., Hannequin, D., Godefroy, O., 2011. Early onset dementia: characteristics in a large cohort from academic memory clinics. Alzheimer Dis. Assoc. Disord. 25, 203–205.
Pruim, R.H., Mennes, M., van Rooij, D., Llera, A., Buitelaar, J.K., Beckmann, C.F., 2015. ICA-AROMA: a robust ICA-based strategy for removing motion artifacts from fMRI data. NeuroImage 112, 267–277.
Rabinovici, G.D., Seeley, W.W., Kim, E.J., Gorno-Tempini, M.L., Rascovsky, K., Pagliaro, T.A., Allison, S.C., Halabi, C., Kramer, J.H., Johnson, J.K., Weiner, M.W., Forman, M.S., Trojanowski, J.Q., Dearmond, S.J., Miller, B.L., Rosen, H.J., 2007. Distinct MRI atrophy patterns in autopsy-proven Alzheimer's disease and frontotemporal lobar degeneration. Am. J. Alzheimers Dis. Other Demen. 22, 474–488.
Rascovsky, K., Salmon, D.P., Ho, G.J., Galasko, D., Peavy, G.M., Hansen, L.A., Thal, L.J., 2002. Cognitive profiles differ in autopsy-confirmed frontotemporal dementia and AD. Neurology 58, 1801–1808.
Rascovsky, K., Hodges, J.R., Knopman, D., Mendez, M.F., Kramer, J.H., Neuhaus, J., van Swieten, J.C., Seelaar, H., Dopper, E.G., Onyike, C.U., Hillis, A.E., Josephs, K.A., Boeve, B.F., Kertesz, A., Seeley, W.W., Rankin, K.P., Johnson, J.K., Gorno-Tempini, M.L., Rosen, H., Prioleau-Latham, C.E., Lee, A., Kipps, C.M., Lillo, P., Piguet, O., Rohrer, J.D., Rossor, M.N., Warren, J.D., Fox, N.C., Galasko, D., Salmon, D.P., Black, S.E., Mesulam, M., Weintraub, S., Dickerson, B.C., Diehl-Schmid, J., Pasquier, F., Deramecourt, V., Lebert, F., Pijnenburg, Y., Chow, T.W., Manes, F., Grafman, J., Cappa, S.F., Freedman, M., Grossman, M., Miller, B.L., 2011. Sensitivity of revised diagnostic criteria for the behavioural variant of frontotemporal dementia. Brain 134, 2456–2477.
Rohde, G.K., Barnett, A.S., Basser, P.J., Marenco, S., Pierpaoli, C., 2004. Comprehensive approach for correction of motion and distortion in diffusion-weighted MRI. Magn. Reson. Med. 51, 103–114.
Rowe, C.C., Ellis, K.A., Rimajova, M., Bourgeat, P., Pike, K.E., Jones, G., Fripp, J., Tochon-Danguy, H., Morandeau, L., O'Keefe, G., Price, R., Raniga, P., Robins, P., Acosta, O., Lenzo, N., Szoeke, C., Salvado, O., Head, R., Martins, R., Masters, C.L., Ames, D., Villemagne, V.L., 2010. Amyloid imaging results from the Australian imaging, biomarkers and lifestyle (AIBL) study of aging. Neurobiol. Aging 31, 1275–1283.
Sajjadi, S.A., Acosta-Cabronero, J., Patterson, K., Diaz-de-Grenu, L.Z., Williams, G.B., Nestor, P.J., 2013. Diffusion tensor magnetic resonance imaging for single subject diagnosis in neurodegenerative diseases. Brain 136, 2253–2261.
Schmidt, R., Verstraete, E., de Reus, M.A., Veldink, J.H., van den Berg, L.H., van den Heuvel, M.P., 2014. Correlation between structural and functional connectivity impairment in amyotrophic lateral sclerosis. Hum. Brain Mapp. 35, 4386–4395.
Serrano, G.E., Sabbagh, M.N., Sue, L.I., Hidalgo, J.A., Schneider, J.A., Bedell, B.J., Van Deerlin, V.M., Suh, E., Akiyama, H., Joshi, A.D., Pontecorvo, M.J., Mintun, M.A., Beach, T.G., 2014. Positive florbetapir PET amyloid imaging in a subject with frequent cortical neuritic plaques and frontotemporal lobar degeneration with TDP43-positive inclusions. J. Alzheimers Dis. 42, 813–821.
Smith, S.M., Nichols, T.E., 2009. Threshold-free cluster enhancement: addressing problems of smoothing, threshold dependence and localisation in cluster inference. NeuroImage 44, 83–98.
Smith, S.M., Jenkinson, M., Woolrich, M.W., Beckmann, C.F., Behrens, T.E., Johansen-Berg, H., Bannister, P.R., De Luca, M., Drobnjak, I., Flitney, D.E., Niazy, R.K., Saunders, J., Vickers, J., Zhang, Y., De Stefano, N., Brady, J.M., Matthews, P.M., 2004. Advances in functional and structural MR image analysis and implementation as FSL. NeuroImage 23 (Suppl. 1), S208–S219.
Smith, S.M., Jenkinson, M., Johansen-Berg, H., Rueckert, D., Nichols, T.E., Mackay, C.E., Watkins, K.E., Ciccarelli, O., Cader, M.Z., Matthews, P.M., Behrens, T.E., 2006. Tract-based spatial statistics: voxelwise analysis of multi-subject diffusion data. NeuroImage 31, 1487–1505.
Smits, L.L., Pijnenburg, Y.A., Koedam, E.L., van der Vlies, A.E., Reuling, I.E., Koene, T., Teunissen, C.E., Scheltens, P., van der Flier, W.M., 2012. Early onset Alzheimer's disease is associated with a distinct neuropsychological profile. J. Alzheimers Dis. 30, 101–108.
Snowden, J.S., Stopford, C.L., Julien, C.L., Thompson, J.C., Davidson, Y., Gibbons, L., Pritchard, A., Lendon, C.L., Richardson, A.M., Varma, A., Neary, D., Mann, D., 2007. Cognitive phenotypes in Alzheimer's disease and genetic risk. Cortex 43, 835–845.
de Souza, L.C., Chupin, M., Bertoux, M., Lehericy, S., Dubois, B., Lamari, F., Le Ber, I., Bottlaender, M., Colliot, O., Sarazin, M., 2013. Is hippocampal volume a good marker to differentiate Alzheimer's disease from frontotemporal dementia? J. Alzheimers Dis. 36, 57–66.
Spinelli, E.G., Mandelli, M.L., Miller, Z.A., Santos-Santos, M.A., Wilson, S.M., Agosta, F., Grinberg, L.T., Huang, E.J., Trojanowski, J.Q., Meyer, M., Henry, M.L., Comi, G., Rabinovici, G., Rosen, H.J., Filippi, M., Miller, B.L., Seeley, W.W., Gorno-Tempini, M.L., 2017. Typical and atypical pathology in primary progressive aphasia variants. Ann. Neurol. 81, 430–443.
Strobl, C., Boulesteix, A.L., Zeileis, A., Hothorn, T., 2007. Bias in random forest variable importance measures: illustrations, sources and a solution. BMC Bioinf. 8, 25.
Strobl, C., Boulesteix, A.L., Kneib, T., Augustin, T., Zeileis, A., 2008. Conditional variable importance for random forests. BMC Bioinf. 9, 307.
Villemagne, V.L., Okamura, N., 2014. *In vivo* tau imaging: obstacles and progress. Alzheimers Dement. 10, S254–S264.
Villemagne, V.L., Furumoto, S., Fodero-Tavoletti, M.T., Mulligan, R.S., Hodges, J., Harada, R., Yates, P., Piguet, O., Pejoska, S., Dore, V., Yanai, K., Masters, C.L., Kudo, Y., Rowe, C.C., Okamura, N., 2014. *In vivo* evaluation of a novel tau imaging tracer for Alzheimer's disease. Eur. J. Nucl. Med. Mol. Imaging 41, 816–826.
Villemagne, V.L., Dore, V., Bourgeat, P., Burnham, S.C., Laws, S., Salvado, O., Masters, C.L., Rowe, C.C., 2017. Abeta-amyloid and tau imaging in dementia. Semin. Nucl. Med. 47, 75–88.
Walterfang, M., Luders, E., Looi, J.C., Rajagopalan, P., Velakoulis, D., Thompson, P.M., Lindberg, O., Ostberg, P., Nordin, L.E., Svensson, L., Wahlund, L.O., 2014. Shape analysis of the corpus callosum in Alzheimer's disease and frontotemporal lobar degeneration subtypes. J. Alzheimers Dis. 40, 897–906.
Wechsler, D., 1987. Wechsler Memory Scale-revised Manual. The Psychological Corporation, San Antonio.
Woolrich, M.W., Jbabdi, S., Patenaude, B., Chappell, M., Makni, S., Behrens, T., Beckmann, C., Jenkinson, M., Smith, S.M., 2009. Bayesian analysis of neuroimaging data in FSL. NeuroImage 45, S173–S186.
Yamauchi, H., Fukuyama, H., Nagahama, Y., Katsumi, Y., Hayashi, T., Oyanagi, C., Konishi, J., Shio, H., 2000. Comparison of the pattern of atrophy of the corpus callosum in frontotemporal dementia, progressive supranuclear palsy, and Alzheimer's disease. J. Neurol. Neurosurg. Psychiatry 69, 623–629.
Zhang, Y., Schuff, N., Du, A.T., Rosen, H.J., Kramer, J.H., Gorno-Tempini, M.L., Miller, B.L., Weiner, M.W., 2009. White matter damage in frontotemporal dementia and

Alzheimer's disease measured by diffusion MRI. Brain 132, 2579–2592.
Zhang, Y., Schuff, N., Ching, C., Tosun, D., Zhan, W., Nezamzadeh, M., Rosen, H.J., Kramer, J.H., Gorno-Tempini, M.L., Miller, B.L., Weiner, M.W., 2011. Joint assessment of structural, perfusion, and diffusion MRI in Alzheimer's disease and frontotemporal dementia. Int. J. Alzheimers Dis. 2011, 546871.
Zhou, J., Greicius, M.D., Gennatas, E.D., Growdon, M.E., Jang, J.Y., Rabinovici, G.D., Kramer, J.H., Weiner, M., Miller, B.L., Seeley, W.W., 2010. Divergent network connectivity changes in behavioural variant frontotemporal dementia and Alzheimer's disease. Brain 133, 1352–1367.
Zhukareva, V., Joyce, S., Schuck, T., Van Deerlin, V., Hurtig, H., Albin, R., Gilman, S., Chin, S., Miller, B., Trojanowski, J.Q., Lee, V.M., 2006. Unexpected abundance of pathological tau in progressive supranuclear palsy white matter. Ann. Neurol. 60, 335–345.